



Delft University of Technology

Slab track-bridge interaction subjected to a moving train an improved matrix formulation and truncation method

Zhang, Qiang; Zhang, Xuehui; Xu, Lei

DOI

[10.1080/23248378.2022.2097134](https://doi.org/10.1080/23248378.2022.2097134)

Publication date

2022

Document Version

Final published version

Published in

International Journal of Rail Transportation

Citation (APA)

Zhang, Q., Zhang, X., & Xu, L. (2022). Slab track-bridge interaction subjected to a moving train: an improved matrix formulation and truncation method. *International Journal of Rail Transportation*, 11(5), 665-684. <https://doi.org/10.1080/23248378.2022.2097134>

Important note

To cite this publication, please use the final published version (if applicable).
Please check the document version above.

Copyright

Other than for strictly personal use, it is not permitted to download, forward or distribute the text or part of it, without the consent of the author(s) and/or copyright holder(s), unless the work is under an open content license such as Creative Commons.

Takedown policy

Please contact us and provide details if you believe this document breaches copyrights.
We will remove access to the work immediately and investigate your claim.



Slab track-bridge interaction subjected to a moving train: an improved matrix formulation and truncation method

Qiang Zhang, Xuehui Zhang & Lei Xu

To cite this article: Qiang Zhang, Xuehui Zhang & Lei Xu (2022): Slab track-bridge interaction subjected to a moving train: an improved matrix formulation and truncation method, International Journal of Rail Transportation, DOI: [10.1080/23248378.2022.2097134](https://doi.org/10.1080/23248378.2022.2097134)

To link to this article: <https://doi.org/10.1080/23248378.2022.2097134>



© 2022 The Author(s). Published by Informa UK Limited, trading as Taylor & Francis Group.



Published online: 12 Jul 2022.



Submit your article to this journal [↗](#)



Article views: 130



View related articles [↗](#)



View Crossmark data [↗](#)

Slab track-bridge interaction subjected to a moving train: an improved matrix formulation and truncation method

Qiang Zhang^a, Xuehui Zhang^b and Lei Xu^{c,d}

^aSchool of Civil Engineering and Architecture, Guangxi University, Nanning, Guangxi, China; ^bDepartment of Geoscience and Engineering, Delft University of Technology, Delft, The Netherlands; ^cDepartment of Railway Engineering, Central South University, Changsha, Hunan, China; ^dNational Engineering Laboratory for High Speed Railway Construction, Central South University, Changsha, Hunan, China

ABSTRACT

Modelling slab track-bridge interaction subject to a moving train usually involves solving complex high-dimensional matrix equations which is time-consuming. This research works to optimize the auto-assembling process in the slab track-bridge coupling matrices formulation and improve the computational efficiency by truncating the dynamic matrices used in time integral scheme. To achieve the above goals, the key issue is to appropriately couple the systems' dynamic matrices in conditions where the elemental sizes of the track slab and the bridge are inconsistent in 3-D space. Besides, by firstly clarifying the degrees of freedom vector of the rail, the track slab and the bridge girder participated in each time step, dynamic matrices characterizing the train-slab track-bridge interaction are truncated with time to reduce the matrix size. This present study has demonstrated the solutions for above problems. Apart from model validations, some numerical examples are presented to show applicability of the proposed methods.

ARTICLE HISTORY

Received 28 January 2022

Revised 28 June 2022

Accepted 29 June 2022

KEYWORDS

Railway engineering dynamics; slab track-bridge interaction; moving train; finite elements model; matrix truncation; numerical simulation

1. Introduction

Bridge structure is widely used in railway engineering, as an elevated rail line can help reduce land occupation and mitigate adverse settlement of rail line compared with on ground embankment. In some rail lines, the bridge length could occupy 80% of the total rail line length or even above, for example the portion of bridge of Beijing-Shanghai High Speed Railway line reaches as high as 86.5%, which indicates the tremendous popularity of bridge in railway engineering [1]. In recent years, high-speed railway has achieved rapid development in China, and slab track system, as the main track system type used in high-speed railway, is widely adopted because of its high stability, less maintenance demand and low structural deformation, etc. From structure viewpoints, the track-bridge system provides fundamental supports to the moving train, and basically influences the train dynamic performance; inversely, the dynamic loading of a moving train deteriorates the track-bridge service performance. Hence it is of great importance to take an in-depth work into the modelling of train-track-bridge interaction.

Compared to the modelling of a train-ballasted track-bridge system [1–6], it is generally a more complex work to depict the slab track-bridge interaction since the track-bridge contact has been changed from the node contact (in ballasted track) to the interface contact, and more complicated plate elements shall be applied instead of beam elements (in ballasted track system). In the

CONTACT Xuehui Zhang  X.Zhang-10@tudelft.nl  Department of Geoscience and Engineering, Delft University of Technology, Delft, The Netherlands

representative work of Zhai et al. [7], the dynamic vibration of the slab tracks is characterized by the mode superposition method (MSM), and the coupled interaction between the slab track and the bridge is characterized by the track-bridge interaction forces. This innovative model is also verified in experiment by Zhai et al. [8], which help provide insights into the complex train-track-bridge system.

Considering the parametric and geometric non-uniformity, nonlinearity, and the modelling efficiency, finite element method (FEM) is generally a more useful tool for track-bridge interaction analysis. Yang et al. [9] made pioneering work on developing vehicle-bridge coupling elements with the proposal of a dynamic condensation method to improve the computational efficiency and stability [10]. Later, Cheng et al [11]. and Lou et al [12]. presented a vehicle-rail-bridge coupling element in the framework of finite element theory. Moreover, Lou et al. [13] developed a modelling method considering the inconsistent length of the rail element and bridge element was developed, where the rail directly connects to the bridge with continuous supports. To analyse the interaction between the rail and the non-uniform continuous bridge, Yang [14] further presented an integrated wheel-rail coupling element using similar approaches as in [9–12]. All these previous studies contribute to a better understanding of track-bridge interaction. However, in the aforementioned work [9–14] on the analysis of track-bridge interaction subject to a moving train, only vertical vibration is modelled where the system lateral vibration was ignored. Besides, for simplicity the wheel-rail elastic compression is mostly neglected [9–12] in the analysis, which was not consistent with practical conditions.

In recent years, train-track-bridge interaction analysis has gained great achievements from the simplified static analysis [15] to the real-time dynamic analysis subjected to a moving train [1–14], and the research dimension has extended from the two-dimensional vertical dynamics analysis [9–14] to the three-dimensional lateral/vertical coupled dynamics analysis [1–5,7,16–20]. In the three-dimensional dynamics model for characterizing the train-track-bridge interaction, Dinh et al. [21] formulated a three-dimensional train-bridge interaction model, where an iterative solution scheme based on Newmark- β method is developed for satisfying the compatibilities at the wheel-rail interfaces. Besides, Zeng and Dimitrakopoulos [22] developed a train-bridge interaction model, where the bridge is modelled by finite element method at 3-D space and the contact-detachment transition along the normal direct of contact is treated as a linear complementarity problem with hypothesis of wheel-rail rigid contacts. However, in the above two studies [21,22], the parametric vibration of the track slab is neglected. Zeng et al. [23] applied the wheel-rail keep-contact method and presented the finite elemental formations for train-track-bridge interaction using energy principle; however, the elemental size of track slab and the bridge is set to be consistent for modelling convenience, which is inconsistent with reality.

From above literature review, it can be cognized that the modelling method and technics for realizing track-bridge interaction analysis have achieved tremendous development within the finite element theory framework. Objectively, the complex slab track-bridge system subjected to a moving train can be built by hybrid modelling of the commercial software, such as ANSYS® and ABAQUS®, etc. However, the general commercial software encounters fatal flaws in the computational efficiency if solving large scale problems. Generally the CPU time consumed at each time integration step is significantly increased by the expansion of the total degrees of freedom (dofs) of the model [24], and in some advanced models the dofs can be as high as above a hundred thousand, which is quite time-consuming.

To improve the computational efficiency while guaranteeing an acceptable precision has been an essential task in advanced train-track-bridge numerical modelling. Accordingly, there are general two possible solutions to this task:

- Reducing the system dofs with a guarantee of the solution precision. Generally the requirement for the finite element size is decreased from the rail, the track slab to the bridge since the main frequency of the substructures is gradually lowered, and accordingly the finite element size can be meshed from fine to coarse level. However, there is co-node and tie-node limits in the commercial software such as ANSYS® and ABAQUS®, causing modelling inconvenience.

- Reducing the matrix size participated in the model solution, i.e., by truncating the matrix and hence reducing the number of dofs involved in the time integral scheme in the case where the boundary effects can be ignored.

Aiming at solving above two issues and accordingly mitigating the modelling deficiency faced in current research, this work develops an improved matrix formulating and truncation method based on previous work. This improved method works effectively to boost the numerical simulation efficiency while assuring a high precision. The rest of this paper is organized as below: in [Section 2](#), the methods for the establishment of the train-track-bridge interaction model are presented, where the improved matrix formulation and truncation methods are introduced and specified; in [Section 3](#), extensive numerical examples are presented to show the application of this proposed model in analysing a series of engineering and parametric problems, followed by a detailed results discussion; in [Section 4](#), conclusions are derived from the numerical studies.

2. Construction of a train-track-bridge interaction model

2.1. Modelling description

A typical train-slab track-bridge system is depicted in [Figure 1](#). In this section, a layered-modelling-method (LMM) [25,26] is introduced and applied to establish the finite-element model of slab track-bridge system. Here, the rail and the bridge girder, the track slab, and the bridge pier are firstly modelled as the Bernoulli-Euler beam, thin-plate and rotatable bar, respectively, and all track structures (rail and slab track) and substructures (bridge girder and pier) are coupled by spring-dashpot elements.

Besides, a train including a series of multi-rigid-body vehicles moves on the track-bridge system, as illustrated in [Figure 2](#). Each vehicle consists of a car body, two bogie frame and four wheel sets, and the rigid bodies are connected by the primary and secondary suspension systems. The wheel-rail

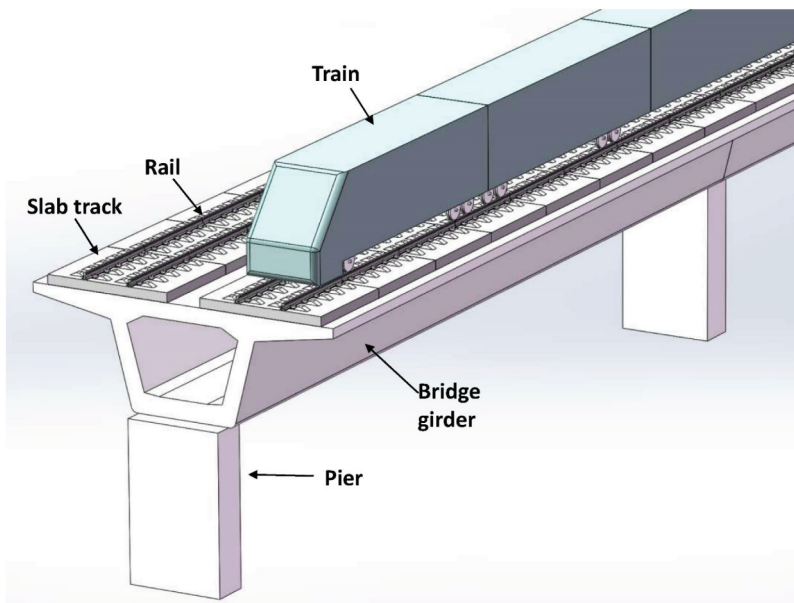


Figure 1. Schematic of a typical train-slab track-bridge system.

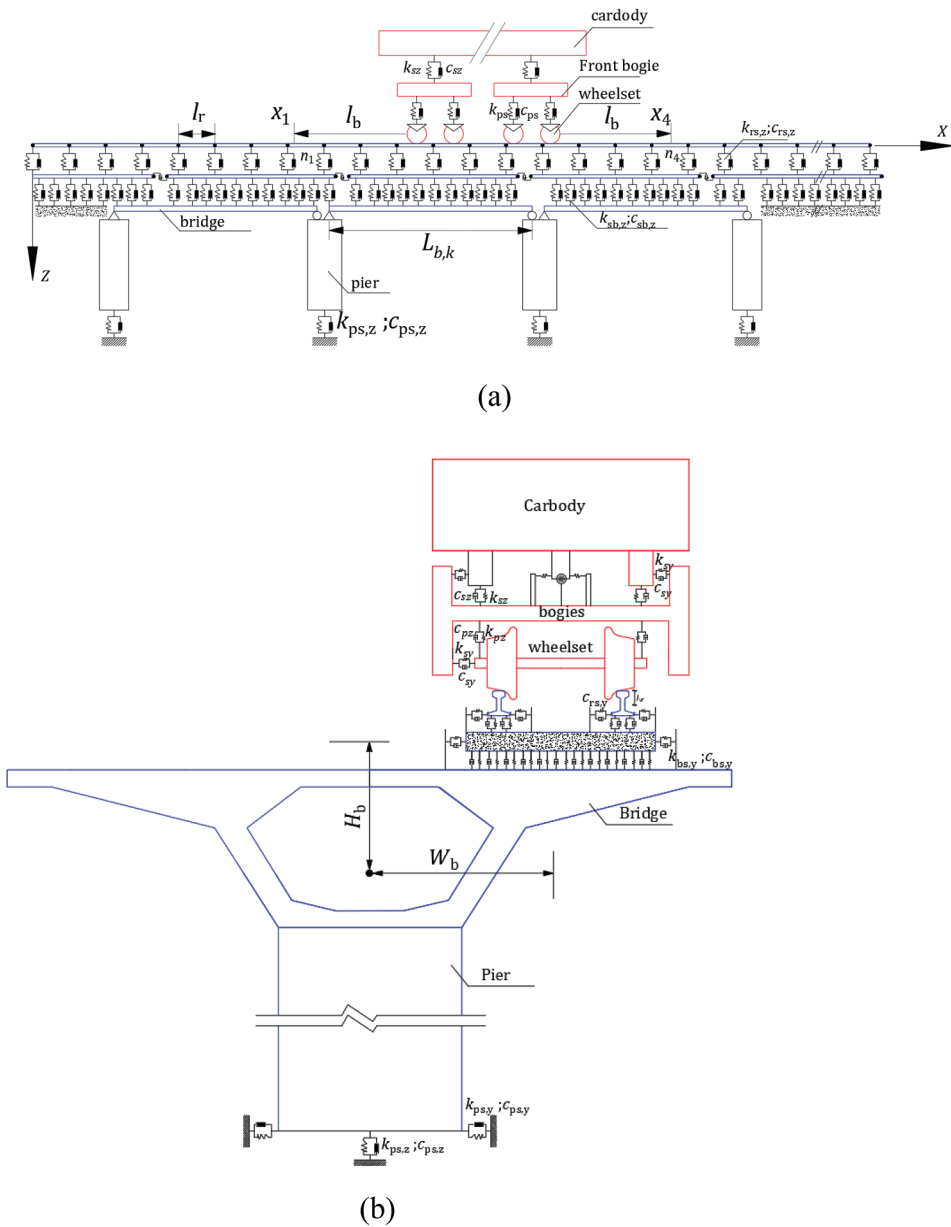


Figure 2. Three-dimensional model for train-track-bridge interaction (a. side view; b. end view).

interaction is characterized by Hertz normal contact, Kalker’s linear creep theory with nonlinear saturated modifications [5], more complete studies on wheel-rail interaction and model coupling can be found in Zhai [27] and Xu [28].

2.2. Matrix formulation of the track-bridge girder interaction

Following methodologies presented in [25,26], the general matrices for the train, the track-substructures, and wheel-rail interactions can be constructed. In this model, the slab track is regarded as the unit slab. When analysing the effects of slab spacing on the system vibration response, the spacing distance is in the range of 100–500 mm in Section 3.2. Therefore, considering

the discontinuity of the track slabs, the difficulty for the automatic assemblage of track slab-bridge girder interaction matrices is dramatically increased because of: (1) the non-equality of elemental length for the track slab at the ends and middle sections (of bridge girder) and (2) the discontinuity of the number of the degrees of freedom (dofs), as shown in [Figure 3](#).

In the derivation of the track slab-bridge girder interaction matrices, i.e., \mathbf{K}_{sb} and \mathbf{C}_{sb} , see for instance, \mathbf{K}_{sb} can be calculated by

$$\mathbf{K}_{sb} = \sum_{i=1}^{N_b} \sum_{j=1}^{n_b} \sum_{\Omega_s} \left(\mathbf{K}_{sb,y}^{i,j,\Omega_s} + \mathbf{K}_{sb,z}^{i,j,\Omega_s} \right) \quad (1)$$

with

$$\mathbf{K}_{sb,y}^{i,j,\Omega_s} = k_{sb,y} \int_{x_1}^{x_2} \mathbf{N}_{sb,y}^T \mathbf{N}_{sb,y} dx \quad (2)$$

$$\mathbf{K}_{sb,z}^{i,j,\Omega_s} = k_{sb,z} \int_0^{w_s} \int_{x_1}^{x_2} \mathbf{N}_{sb,z}^T \mathbf{N}_{sb,z} dx dy \quad (3)$$

with

$$\begin{cases} \mathbf{N}_{sb,y} = [\mathbf{V}_s & -\bar{\mathbf{V}}_b] \\ \mathbf{N}_{sb,z} = [\mathbf{W}_s & -\bar{\mathbf{W}}_b] \end{cases} \quad (4)$$

$$\mathbf{W}_s = [N_1^s \mathbf{N}_{s,z} \quad N_2^s \mathbf{U}_s \quad N_3^s \mathbf{N}_{s,z} \quad N_4^s \mathbf{U}_s] \quad (5)$$

$$\begin{cases} N_1^s = 1 - 3\zeta^2 + 2\zeta^3 \\ N_2^s = -(\zeta - 2\zeta^2 + \zeta^3)w_s \\ N_3^s = 3\zeta^2 - 2\zeta^3 \\ N_4^s = -(\zeta^3 - \zeta^2)w_s \end{cases} \quad (6)$$

where $\zeta = \frac{y}{w_s}$, and

$$\begin{cases} \mathbf{N}_{s,z} = [N_1^s & N_2^s & N_3^s & N_4^s] \\ \mathbf{U}_s = [1 - \zeta & \zeta] \end{cases} \quad (7)$$

where $\zeta = \frac{x}{l_s}$, and

$$\bar{\mathbf{W}}_b = [\mathbf{N}_{b,z} \quad (W_b - \frac{w_s}{2} + y)\mathbf{U}_b] \quad (8)$$

$$\begin{cases} \mathbf{N}_{b,z} = [N_1^b & N_2^b & N_3^b & N_4^b] \\ \mathbf{U}_b = [N_1^U & N_2^U] \end{cases} \quad (9)$$

where

$$\begin{cases} N_1^b = 1 - 3\bar{\xi}^2 + 2\bar{\xi}^3 \\ N_2^b = -(\bar{\xi} - 2\bar{\xi}^2 + \bar{\xi}^3)l_{tb} \\ N_3^b = 3\bar{\xi}^2 - 2\bar{\xi}^3 \\ N_4^b = -(\bar{\xi}^3 - \bar{\xi}^2)l_{tb} \\ N_1^U = 1 - \bar{\xi} \\ N_2^U = \bar{\xi} \end{cases} \quad (10)$$

where $\bar{\xi} = \frac{l_x + x}{l_{tb}}$, and

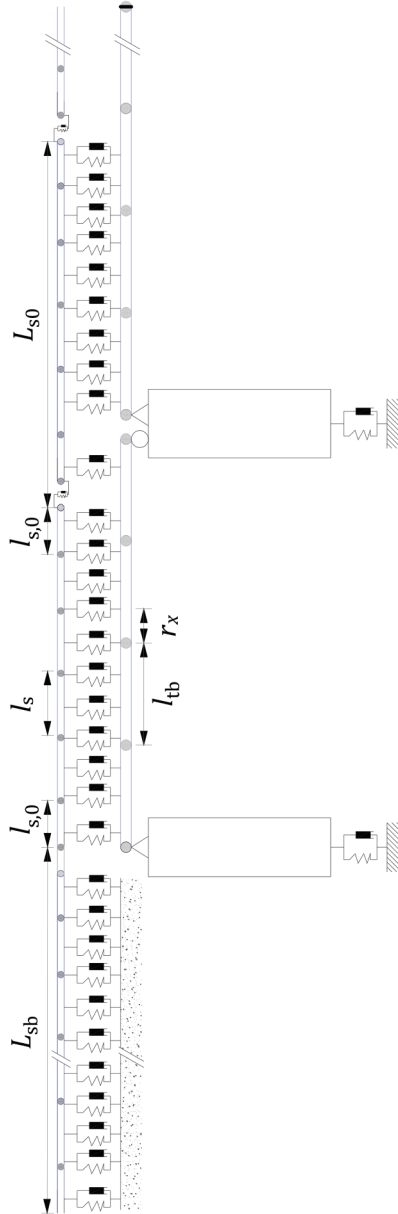


Figure 3. A schematic of the track slab-bridge interaction with discontinuity of the elemental length.

$$\begin{cases} \mathbf{V}_s = [N_1^s & -N_2^s & N_3^s & -N_4^s] \\ \bar{\mathbf{V}}_b = [\mathbf{N}_{b,y} & H_b \mathbf{U}_b] \\ \mathbf{N}_{b,y} = [N_1^b & -N_2^b & N_3^b & -N_4^b] \end{cases} \quad (11)$$

where $k_{sb,y}$ and $k_{sb,z}$ denote respectively the track slab-girder lateral and vertical interaction stiffness; w_s and l_s are respectively the width and the length of the track slab along the Y - and X - axis direction (see Figure 3(a)); H_b and W_b are respectively the vertical and lateral distance between the girder centroid and the centroid of the track slab (see Figure 3(b)); l_{tb} is the beam elemental length of the girder; N_b is the total number of bridge spans and n_b is the total number of the finite elements for each girder; x_1 and x_2 indicate the lower and upper boundary of slab-bridge interaction area, respectively; r_x means the distance between the slab element (front node) and the bridge element (front node), see Figure 3; Ω_s is the assemblage of the track slab element number contacting with the n_b -th girder element at the N_b -th span; \mathbf{W}_s denotes the shape function describing the vertical motion of a track slab as a thin-plate element and \mathbf{V}_s denotes the shape function describing the lateral motion of the track slab as a beam element; \mathbf{W}_b and \mathbf{V}_b denote respectively the shape function for vertical and lateral motion description of a bridge girder as a beam element.

From Equations (1) to (3), it can be seen that it is highly important to confirm the parameters Ω_s , r_x , x_1 and x_2 . The steps below can be followed to obtain these parameters:

1) Calculate the longitudinal location of the start and end node for a bridge girder element at the bridge coordinate system, that is,

$$\begin{cases} X_{b,1} = (N_b - 1)l_{br} + L_{br,N_b} + (n_b - 1)l_{tb} \\ X_{b,2} = (N_b - 1)l_{br} + L_{br,N_b} + n_b l_{tb} \end{cases} \quad (12)$$

where l_{br} is the spacing between bridge girders; $L_{br,i}$ is the sum length of bridge girders before the N_b -th span; l_{tb} is the length of the bridge beam element; $X_{b,1}$ and $X_{b,2}$ are the start and the end position of the girder beam element respectively.

2) Calculate the longitudinal start and end locations for the track slab thin-plate elements at the track slab coordinate system, that is,

$$\begin{cases} X_{s,1} = X_{b,1} + L_{sb} \\ X_{s,2} = X_{b,2} + L_{sb} \end{cases} \quad (13)$$

where L_{sb} is the total length of the track slabs before the starting of the bridge.

3) To confirm Ω_s , here three sub steps are followed as:

Sub-step 1: confirm the number for the track slab

$$\begin{cases} i_1 = \Upsilon \left[\frac{X_{s,1}}{L_{s0}} \right] + 1 \\ L'_{s1} = X_{s,1} - (i_1 - 1)L_{s0} \\ i_2 = \Upsilon \left[\frac{X_{s,2}}{L_{s0}} \right] + 1 \\ L'_{s2} = X_{s,2} - (i_2 - 1)L_{s0} \end{cases} \quad (14)$$

where i_1 denotes the i_1 -th track slab and i_2 denotes the i_2 -th track slab; L_{s0} is the length of a track slab; $\Upsilon[\cdot]$ denotes the operator rounded the element to the nearest integer towards zero.

Sub-step 2: confirm the elemental number for the i_1 -th and the i_2 -th track slab

$$n_{s1} = \begin{cases} 1 & \text{if } L'_{s1} < l_{s,0} \\ n_{s1,0} + 2 & \text{if } L'_{s1} \geq (l_{s,0} + n_{s1,0}l_s) \\ \Upsilon[(L'_{s1} - l_{s,0})/l_s] + 2 & \text{else} \end{cases} \quad (15)$$

$$n_{s2} = \begin{cases} 1 & \text{if } L'_{s2} < l_{s,0} \\ n_{s1,0} + 2 & \text{if } L'_{s2} \geq (l_{s,0} + n_{s1,0}l_s) \\ Y[(L'_{s2} - l_{s,0})/l_s] + 2 & \text{else} \end{cases} \quad (16)$$

where n_{s1} and n_{s2} denotes the elemental number with respect to the i_1 -th and the i_2 -th track slab; $n_{s1,0}$ is the total number of track slab elements between two end elements of a track slab, and each track slab element has an elemental length of l_s ;

Sub-step 3: determine the track slab elements contacting with the bridge girder element

$$\Omega_s = \begin{cases} (n_{s1}, n_{s1} + 1, \dots, n_{s2}) & \text{if } i_1 = i_2 \\ (n_{s1}, n_{s1} + 1, \dots, n_{s1,0} + 2, 1, 2, \dots, n_{s2}) & \text{if } i_1 < i_2 \end{cases} \quad (17)$$

Corresponding to Ω_s , an assemblage of the track slab number each track slab with length of L_{s0} can be obtained by

$$\tilde{\Omega}_s = \begin{cases} (i_1, i_1, \dots, i_1) \\ (i_1, i_1, \dots, i_1, i_2, i_2, \dots, i_2) \end{cases} \quad (18)$$

Sub-step 4: confirm parameters of r_x , x_1 and x_2 according to the following judgement:

First, the start and end position of a track slab element can be obtained by

$$X_{s,1} = \begin{cases} L_{s0}(\tilde{\Omega}_s(q) - 1) & \text{if } \Omega_s(q) = 1 \\ L_{s0}(\tilde{\Omega}_s(q) - 1) + l_{s,0} + l_s(\Omega_s(q) - 2) & \text{if } \Omega_s(q) > 1 \text{ or } \Omega_s(q) < n_{s1,0} + 2 \\ L_{s0}\tilde{\Omega}_s(q) - l_{s,0} & \text{if } \Omega_s(q) = (n_{s1,0} + 2) \end{cases} \quad (19)$$

$$X_{s,2} = \begin{cases} L_{s0}(\tilde{\Omega}_s(q) - 1) + l_{s,0} & \text{if } \Omega_s(q) = 1 \\ L_{s0}(\tilde{\Omega}_s(q) - 1) + l_{s,0} + l_s(\Omega_s(q) - 1) & \text{if } \Omega_s(q) > 1 \text{ or } \Omega_s(q) < (n_{s1,0} + 2) \\ L_{s0}\tilde{\Omega}_s(q) - d_{vv} & \text{if } \Omega_s(q) = (n_{s1,0} + 2) \end{cases} \quad (20)$$

where q denotes the q -th number in the assembled set of $\tilde{\Omega}_s$ or Ω_s .

Second, the start and end positions of a bridge girder beam element have been obtained in Equation (2), and finally the method for deriving the parameters r_x , x_1 and x_2 can be got by

$$r_x = X_{s,1} - X_{b,1} \quad (21)$$

$$x_1 = \begin{cases} 0 & \text{if } X_{s,1} \geq X_{b,1} \\ X_{b,1} - X_{s,1} & \text{if } X_{s,1} < X_{b,1} \end{cases} \quad (22)$$

$$x_2 = \begin{cases} \bar{l}_s - (X_{s,2} - X_{b,2}) & \text{if } X_{s,1} \geq X_{b,1} \text{ and } X_{s,2} \geq X_{b,2} \\ \bar{l}_s & \text{if } X_{s,2} < X_{b,2} \end{cases} \quad (23)$$

with

$$\bar{l}_s = \begin{cases} l_{s,0} & \text{if } \Omega_s(q) = 1 \text{ or } \Omega_s(q) = n_{s1,0} + 2 \\ l_s & \text{else} \end{cases} \quad (24)$$

and the programme will display 'error' if $X_{s,1} \leq X_{b,1}$ and if $X_{s,2} \geq X_{b,2}$, indicating that the bridge girder elemental length is smaller than the length of a track slab element.

Through above derivations, all parameters used in Equation (1) can be obtained properly.

2.3. The dynamic equations of motion for train-track-bridge interaction

By matrix formulations, the dynamic equations of motion for train-track-bridge interactions can be assembled by

$$\begin{bmatrix} \mathbf{M}_{tt} & \mathbf{0} & \mathbf{0} & \mathbf{0} & \mathbf{0} \\ \mathbf{0} & \mathbf{M}_{rr} & \mathbf{0} & \mathbf{0} & \mathbf{0} \\ \mathbf{0} & \mathbf{0} & \mathbf{M}_{ss} & \mathbf{0} & \mathbf{0} \\ \mathbf{0} & \mathbf{0} & \mathbf{0} & \mathbf{M}_{bb} & \mathbf{0} \\ \mathbf{0} & \mathbf{0} & \mathbf{0} & \mathbf{0} & \mathbf{M}_{pp} \end{bmatrix} \begin{Bmatrix} \ddot{\mathbf{X}}_t \\ \ddot{\mathbf{X}}_r \\ \ddot{\mathbf{X}}_s \\ \ddot{\mathbf{X}}_b \\ \ddot{\mathbf{X}}_p \end{Bmatrix} + \begin{bmatrix} \mathbf{C}_{tt} & \mathbf{C}_{tr} & \mathbf{0} & \mathbf{0} & \mathbf{0} \\ \mathbf{C}_{rt} & \mathbf{C}_{rr} & \mathbf{C}_{rs} & \mathbf{0} & \mathbf{0} \\ \mathbf{0} & \mathbf{C}_{sr} & \mathbf{C}_{ss} & \mathbf{C}_{sb} & \mathbf{0} \\ \mathbf{0} & \mathbf{0} & \mathbf{C}_{bs} & \mathbf{C}_{bb} & \mathbf{C}_{bp} \\ \mathbf{0} & \mathbf{0} & \mathbf{0} & \mathbf{C}_{pb} & \mathbf{C}_{pp} \end{bmatrix} \begin{Bmatrix} \dot{\mathbf{X}}_t \\ \dot{\mathbf{X}}_r \\ \dot{\mathbf{X}}_s \\ \dot{\mathbf{X}}_b \\ \dot{\mathbf{X}}_p \end{Bmatrix} + \begin{bmatrix} \mathbf{K}_{tt} & \mathbf{K}_{tr} & \mathbf{0} & \mathbf{0} & \mathbf{0} \\ \mathbf{K}_{rt} & \mathbf{K}_{rr} & \mathbf{K}_{rs} & \mathbf{0} & \mathbf{0} \\ \mathbf{0} & \mathbf{K}_{sr} & \mathbf{K}_{ss} & \mathbf{K}_{sb} & \mathbf{0} \\ \mathbf{0} & \mathbf{0} & \mathbf{K}_{bs} & \mathbf{K}_{bb} & \mathbf{K}_{bp} \\ \mathbf{0} & \mathbf{0} & \mathbf{0} & \mathbf{K}_{pb} & \mathbf{K}_{pp} \end{bmatrix} \begin{Bmatrix} \mathbf{X}_t \\ \mathbf{X}_r \\ \mathbf{X}_s \\ \mathbf{X}_b \\ \mathbf{X}_p \end{Bmatrix} = \begin{Bmatrix} \mathbf{F}_t \\ \mathbf{F}_r \\ \mathbf{0} \\ \mathbf{0} \\ \mathbf{0} \end{Bmatrix} \quad (25)$$

where \mathbf{M} , \mathbf{C} and \mathbf{K} denote the mass, damping and stiffness matrices respectively; the subscript 't', 'r', 's', 'b' and 'p' denote the train, the rail, the track slab, the bridge girder and the pier respectively; \mathbf{X} , $\dot{\mathbf{X}}$ and $\ddot{\mathbf{X}}$ are respectively the displacement, velocity and acceleration vector respectively; \mathbf{F} denotes the loading vector.

In Equation (25), the entire track-bridge system subject to a moving train has been characterized in a matrix coupling way. The wheel-rail interaction matrices ' \mathbf{C}_{tr} ', ' \mathbf{C}_{rt} ', ' \mathbf{K}_{tr} ' and ' \mathbf{K}_{rt} ' are time-dependent following the change of wheel-rail contact positions and possess nonlinearity. For such a complex system, direct time integration algorithm such as Newmark- β method can be used to obtain the system responses.

2.4. Matrix truncation method for improving the model solution efficiency

For a model constructed by finite elements, it generally possesses high degrees of freedom (dofs) if the slab track and the bridge system are very long or with small finite elemental sizes, which usually results in an extremely large size of dynamic matrices. Therefore, the computational efficiency will be significantly decreased by the large-scale size of the dynamic matrices participated in the time domain integration.

In the model solution, the track-bridge coupling matrices are truncated to reduce the matrix dofs in the numerical integration to improve the computational efficiency. The hidden criteria or philosophy for truncation is to properly locate the boundary where the boundary effects are quite small as to be ignored in modelling, and the algorithm for boundary truncation is described in detail in below sections.

2.4.1. Rail dofs vector

The start and end dof for the rail system can be respectively obtained as

$$\begin{cases} \delta_{r,1} = \Psi_r(n_1 - 1) + 1 \\ \delta_{r,4} = \Psi_r(n_4 + 1) \end{cases} \quad (26)$$

with

$$\begin{cases} n_1 = \Upsilon[x_1/l_r] + 1 \\ n_4 = \Upsilon[x_4/l_r] + 1 \end{cases} \quad (27)$$

where Ψ_r is half of the dofs for a rail beam element; n_1 and n_4 are the rail beam number where the first and the fourth wheelset contact with the rail, as shown in [Figure 2\(a\)](#); x_1 and x_4 denote the boundary positions at the X -axis; l_r is the distance between adjacent rail pads.

The rail dofs vector can be obtained as $\delta_r = [\delta_{r,1}, \delta_{r,4}]$.

2.4.2. Track slab dofs vector

The start and end dof for the track slab system can be respectively obtained as

$$\begin{cases} \delta_{s,1} = (3(n_w + 1) + 2)(i_1 - 1) + \Psi_s(I_1 - 1) + 1 \\ \delta_{s,4} = (3(n_w + 1) + 2)(i_4 - 1) + \Psi_s(I_4 + 1) \end{cases} \quad (28)$$

With

$$\begin{cases} i_1 = Y[x_1/L_{s0}] + 1 \\ i_4 = Y[x_4/L_{s0}] + 1 \end{cases} \quad (29)$$

$$I_1 = \begin{cases} 1 & \text{if } \bar{x}_1 < l_{s,0} \\ n_{s1,0} + 2 & \text{if } \bar{x}_1 \geq l_{s,0} + n_{s1,0}l_s \\ Y[\bar{x}_1/l_s] + 1 & \text{else} \end{cases} \quad (30)$$

$$I_4 = \begin{cases} 1 & \text{if } \bar{x}_4 < l_{s,0} \\ n_{s1,0} + 2 & \text{if } \bar{x}_4 \geq l_{s,0} + n_{s1,0}l_s \\ Y[\bar{x}_4/l_s] + 1 & \text{else} \end{cases} \quad (31)$$

$$\begin{cases} \bar{x}_1 = x_1 - L_{s0}(i_1 - 1) \\ \bar{x}_4 = x_4 - L_{s0}(i_4 - 1) \end{cases} \quad (32)$$

where n_w is the lateral divisions for a track slab; i_1 and i_4 denote the track slab number with respect to locations x_1 and x_4 ; I_1 and I_4 denote the plate elements at the i_1 -th and the i_4 -th track slab respectively.

The track slab dofs vector can be obtained as $\delta_s = [\delta_{s,1}, \delta_{s,4}]$.

2.4.3. Bridge dofs vector

The start and end dof for the bridge system can be respectively obtained as

$$\begin{cases} \delta_{b,1} = \bar{\Psi}_{b,i} + \Psi_b(n_{b,1} - 1) + 1 \\ \delta_{b,4} = \bar{\Psi}_{b,j} + \Psi_b(n_{b,4} + 1) \end{cases} \quad (33)$$

With

$$\begin{cases} \bar{\Psi}_{b,i} = \Psi_b \sum_i (n_{b,i} - 1) + 2i\Psi_b - (\Psi_b(n_{b,i} - 1) + 2\Psi_b) \\ \bar{\Psi}_{b,j} = \Psi_b \sum_j (n_{b,j} - 1) + 2j\Psi_b - (\Psi_b(n_{b,j} - 1) + 2\Psi_b) \end{cases} \quad (34)$$

$$n_{b,1} = \begin{cases} Y[l_{b,1}/l_{tb}] + 1 & \text{if } l_{b,1} < L_{b,i} \\ n_{b,i} & \text{else} \end{cases} \quad (35)$$

$$n_{b,4} = \begin{cases} Y[l_{b,4}/l_{tb}] + 1 & \text{if } l_{b,4} < L_{b,i} \\ n_{b,j} & \text{else} \end{cases} \quad (36)$$

$$l_{b,1} = \begin{cases} \tilde{x}_1 & \text{if } i = 1 \\ \tilde{x}_1 - \sum_{k=1}^{i-1} L_{b,k} - l_{br}(i-1) & \text{else} \end{cases} \quad (37)$$

$$l_{b,4} = \begin{cases} \tilde{x}_4 & \text{if } j = 1 \\ \tilde{x}_4 - \sum_{k=1}^{j-1} L_{b,k} - l_{br}(j-1) & \text{else} \end{cases} \quad (38)$$

where the symbols ‘ i ’ and ‘ j ’ denote the i -th and the j -th bridge girder; Ψ_b denotes half of the dofs for a girder beam element; $\bar{\Psi}_{b,i}$ and $\bar{\Psi}_{b,j}$ denote the total dofs of the girders before the i -th and the j -th bridge girder; $n_{b,1}$ and $n_{b,4}$ denote the element number for the start and end bridge girder; $L_{b,i}$ and $L_{b,j}$ denote the bridge girder length for the i -th and the j -th bridge girder; \tilde{x}_1 and \tilde{x}_4 denote the boundary positions at the bridge coordinate; $L_{b,k}$ is the bridge girder length for the k -th girder.

The bridge dofs vector can be obtained as $\delta_b = [\delta_{b,1}, \delta_{b,4}]$. Because the dofs of the piers δ_p are relatively less, they are fully considered in the simulation.

In Summary, the dofs used in the time integration is assembled as

$$\delta = [\delta_r \quad \delta_s \quad \delta_b \quad \delta_p] \quad (39)$$

2.5. Model comparisons

In this example, a previous model presented in [28], where the wheel and the rail are regarded as rigid contacts, is introduced and compared as a validation (of the model in this study). In this model, the wheel-rail geometric relationship is obtained by the track line method. Moreover, the matrix coupling method based on the Hertz nonlinear theory and saturated creep theory is used to construct the interaction matrix between the wheel and rail. The detailed parameters in this model, including the bridge, track slab and the vehicle are listed in Table A1 and A2 in Appendix. Also, the irregularity excitation function is presented in Figure 4.

Figure 5 shows the comparison on bridge vertical and lateral accelerations at the bridge mid-span between these two models, from which it can be observed that the bridge accelerations of these two models excited by track random irregularities coincide very well with each other and accordingly the effectiveness of this model has been validated. Besides, the comparison on car body acceleration has also been illustrated in Figure 6. It can be seen that the response curve of car body accelerations agrees well to each other, and the response amplitudes are a little different due to the difference of the wheel-rail coupling flexibility in the rigid- and elastic-contact scenarios.

3. Numerical studies

In the numerical studies, three examples will be presented: the first example is to investigate the influence of track slab element types on system responses; the second example discusses the influence of the discontinuity of track slabs on system responses and the last example is to show the influence of matrix boundary truncation length on system responses.

In the numerical solutions, it is assumed a train consisting of three identical vehicles moves on the simply supported bridge, the time step interval is set 0.24 ms, while the moving speed (of the train) is 300 km/h.

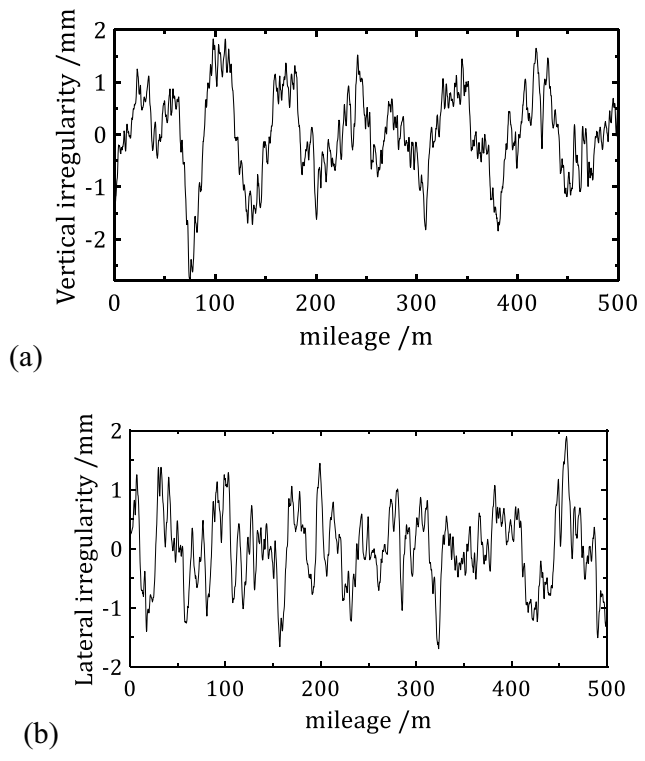


Figure 4. Track irregularity ((a). vertical; (b) lateral).

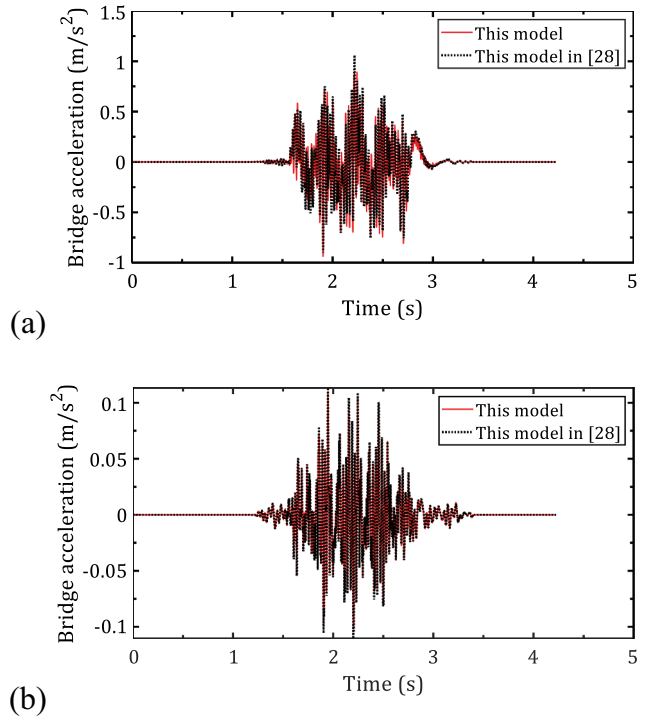


Figure 5. Comparison on bridge acceleration at the mid-span (a. vertical acceleration; b. lateral acceleration).

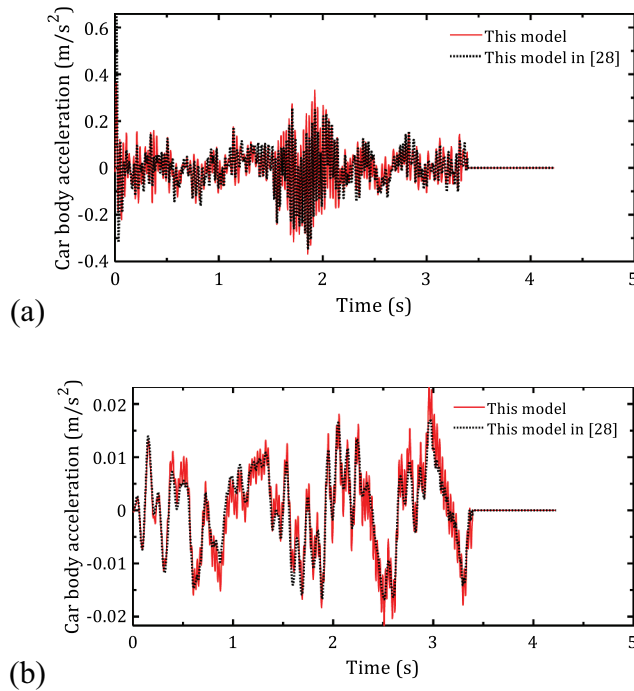


Figure 6. Comparison on car body acceleration at the mid-span (a. vertical acceleration; b. lateral acceleration).

3.1. Influence of track slab element types on system responses

Conventionally thin-plate element is applied to model the track slab system but its engineering practicality comparing to other finite element types is rarely reported. In this study three types of finite elements, i.e., double-beam, thin-plate and Mindlin-Reissner plate, are introduced to model the track slabs. The finite element size of the track slab is set to be with the longitudinal length of 0.325 m and the lateral width of 0.343 m.

Figure 7 shows the track slab vertical acceleration with respect to different plate element types. It can be observed from Figure 7(a) that the response curve of the double beam element is highly consistent to that of the thin-plate element, but the response corresponding to the Mindlin-Reissner plate element is generally smaller than those of the double beam and thin plate, i.e., the track slab vertical acceleration is lower when considering the shearing deformation of the track slab in the Mindlin-Reissner plate element, and the maximum acceleration difference between those of the double element/ thin plate elements and the Mindlin-Reissner reaches $2 m/s^2$. Besides, Figure 7(b) further presents the power spectral density (PSD) distribution of the track slab vertical acceleration with respect to various plate elements, from which it can be seen that all PSD curves against different element types coincide well within the frequency 83.41 Hz, above which the frequency response differences start to emerge between the elemental types, similarly the frequency response of the Mindlin-Reissner at specific high frequency ranges (>83.41 Hz) is generally smaller than those of the double beam and the thin plate.

Moreover Figure 8 shows the influence of track slab element type on bridge acceleration, from which it can be observed that the track slab element type shows relatively slight influence on bridge acceleration, as the bridge accelerations (corresponding to the three element types) shows very small difference. Also, it is found that the bridge acceleration attached to the Mindlin-Reissner plate element is generally smaller than those attached to the elements of double beam and thin plate with a maximum difference of $0.05 m/s^2$, besides the differences between them mainly occur at the frequency range of above 140.4 Hz.

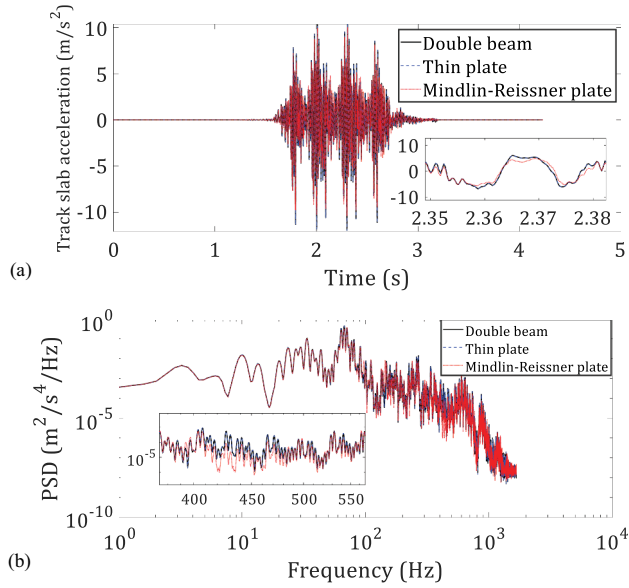


Figure 7. Track slab vertical acceleration at the mid-span of the bridge (a. time-domain response; b. frequency-domain PSD response).

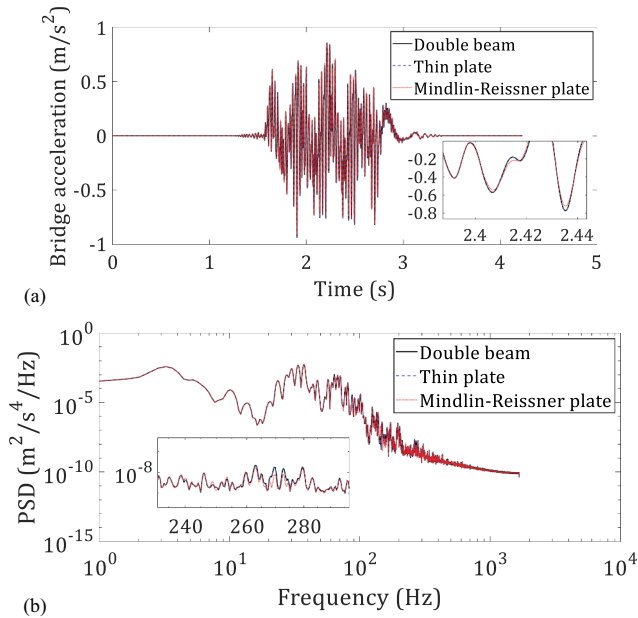


Figure 8. Bridge vertical acceleration at the mid-span of the bridge (a. time-domain response; b. frequency-domain PSD response).

3.2. Influence of the discontinuity of track slabs on system responses

For various slab track systems, the physical configuration of the track slabs is different, e.g., some are longitudinally discontinuous with track slab spacing, such as the I series and III series track slab of China Railway Track System (referred as CRTS-I and CRTS-III type track slab), some are longitudinally connected such as II series track slab of China Railway Track System (referred as CRTS-II type).

To clarify the influence of the discontinuity of track slabs on system dynamic performance, this subsection considers the spacing of adjacent track slabs, denoted as l_{ss} , to be varied from 0.1 m to 0.50 in the discontinuous track slab system, besides the longitudinally connected track slab system is modelled as continuous track slabs, denoted as l_{ss}^0 . The train speed is set to be 300 km/h.

To clearly illustrate the influence of the discontinuity of the track slab, the additional effects of track irregularities are ignored here. Figure 9 shows the time-varying displacement of the rail and the bridge, and the wheel-rail vertical force beneath first wheelset of the moving train. It can be observed from Figure 9 that the maximum responses of all dynamic indices are gradually increased by the increase of the track slab spacing, and the maximum responses are increased by 2.5%, 1.3% and 1.7% for indices of rail displacement, bridge displacement and the wheel-rail force respectively. What's more, it can be seen that the presented dynamic responses subject to longitudinally connected (continuous) track slabs are smaller than those subject to discontinuous track slabs.

Figure 10 shows the power spectral densities (PSD) against time domain wheel-rail forces. It can be observed from Figure 10 that the geometric features of the track-bridge systems have been clearly revealed, such as the rail pad spacing, discontinuity of track slab and bridge span length that cause the periodicity of support stiffness. Besides it can be observed that the characteristic wavelength of the track slab length is not appeared in the continuous track slabs due to the longitudinal connection of the track slabs. In summary, influence of the discontinuity of track slabs on system responses are successfully revealed with the model in this study.

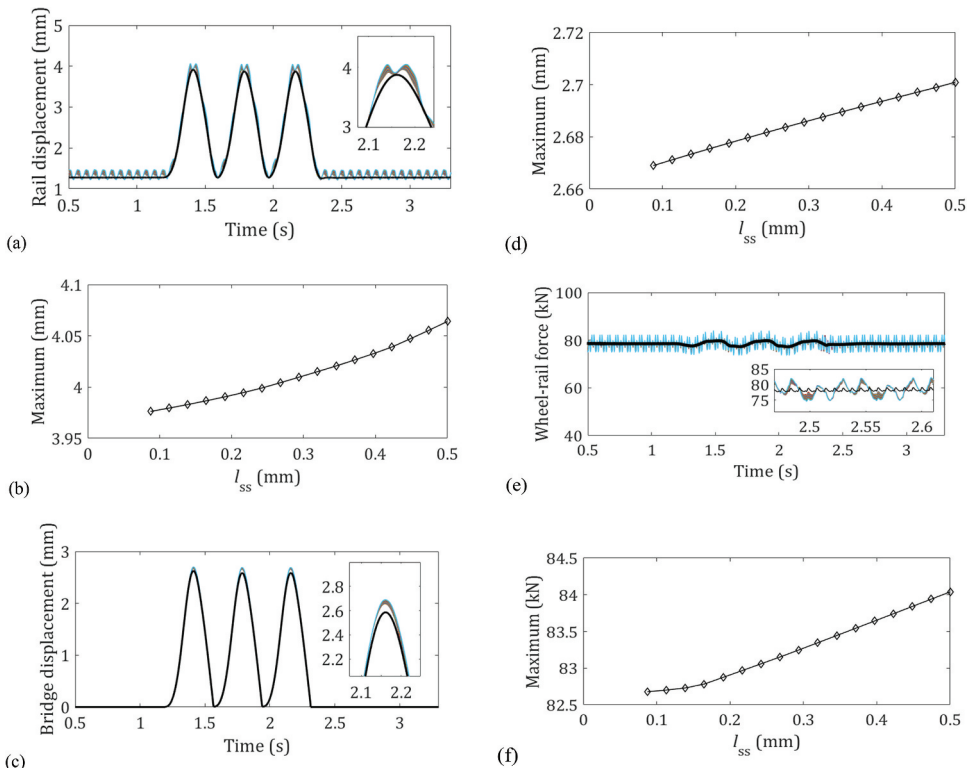


Figure 9. Influence of discontinuity of track slabs against different values of l_{ss} (a-b. rail displacement; c-d. bridge displacement; e-f. wheel-rail vertical force) (the black solid line indicates the time-domain responses against longitudinally connected track slabs).

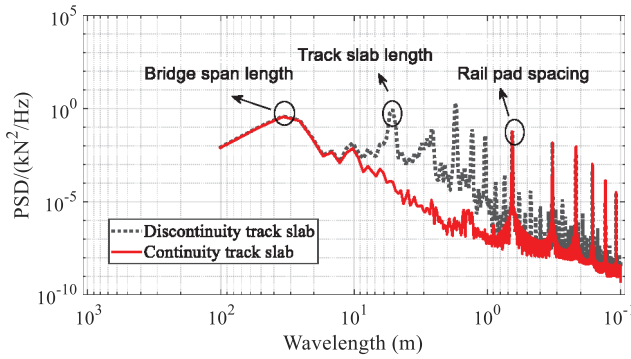


Figure 10. Power spectral density distribution of wheel-rail vertical force against track slab types.

3.3. Determination of the boundary length on system performance

In this model, the train-track-bridge coupling matrices are truncated at the boundary as described in section 2.4, so as to improve the computational efficiency. However, it is widely known there exists structural wave propagation and reflection from boundaries, and thus it is significantly important to confirm the minimum boundary length of l_b , above which length the wave reflection effects can be neglectable.

As shown in Figure 11, different length of l_b is selected and the bridge accelerations with respect to various l_b are presented, from which it can be observed that the vibration fluctuation at the boundary section are significantly more violent than others if the boundary length is small such as $l_b=10\text{m}$. More specifically, set l_b to be varied from 10 m to 50 m and the span width of the simply supported bridge to be 20 m and 32 m, and Figures 12, 13 shows the normalized maximum rail and bridge vibration (by dividing the maximum responses) with respect to various boundary lengths.

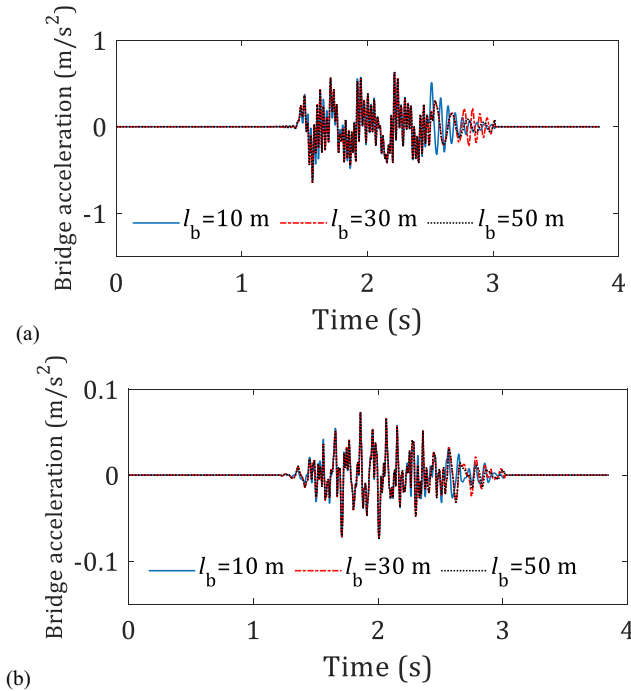


Figure 11. Effects of the boundary length on bridge acceleration at the mid-span (a. bridge vertical acceleration; b. bridge lateral acceleration).

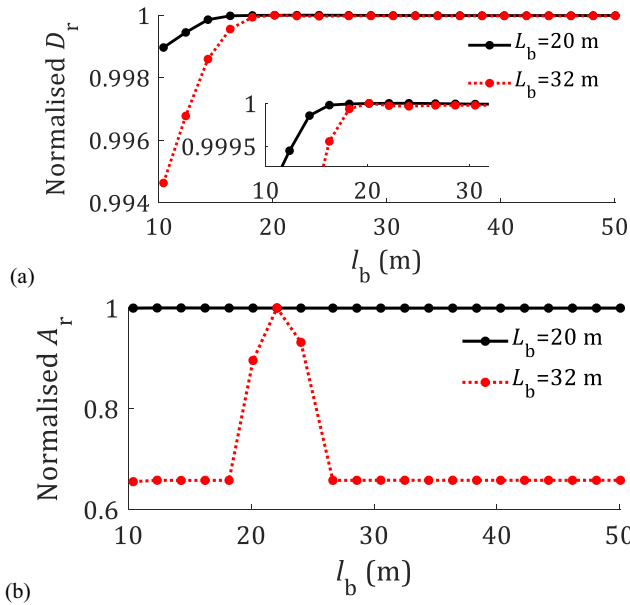


Figure 12. The maximum rail vibration with respect to different boundary lengths (a. rail vertical displacement; b. rail vertical acceleration).

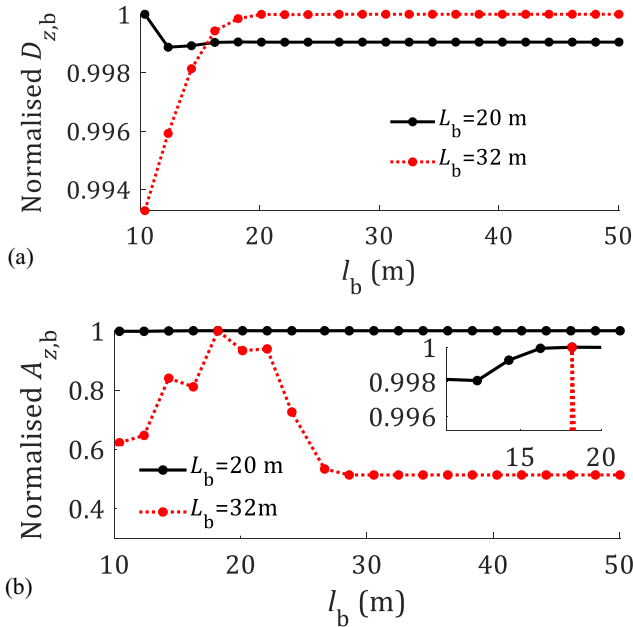


Figure 13. The maximum bridge vibration with respect to different boundary lengths (a. bridge vertical displacement; b. bridge vertical acceleration).

It can be clearly seen from [Figure 12](#) that the shorter of the bridge span length, the smaller of the boundary length required, in the guaranteeing of the solution convergence. See for instance, the rail vibration is almost unchanged when l_b is larger than 20 m and 32 m, namely the boundary length distance from the front and rear of the wheelset should be larger than the span length of the simply supported

bridge. Figure 13 has further presented the normalized values of the bridge maximum vertical displacement and acceleration, from which it can be also noticed that the bridge vertical vibrations are gradually converged to specific values once $l_b > L_b$, where L_b is the bridge span length.

By selecting the minimum boundary length l_b , the time consumption is greatly reduced in the modelling solution. For example, in scenario of minimum boundary length (the l_b is set 10 m), the CPU (typed Intel(R) Core(TM) i7-10700K-3.80 GHz) time is respectively 321 seconds and 1680 seconds for the solutions considering and not considering the matrix boundary truncation.

4. Conclusions

In this paper an improved modelling method for characterizing slab track-bridge interaction subject to a moving train is proposed, where an innovative matrix truncation method is developed to improve the computational efficiency. The technologically advanced aspects of this model lie in automatically assembling slab track-bridge coupling matrices with inconsistent finite element sizes and detail formula of key parameters.

Apart from the model validations, some conclusions can be drawn from the numerical studies:

(1) The double-beam and thin-plate elements have close precision in depicting the dynamic behaviours of track slabs. With consideration of the shear deformation, Mindlin-Reissner plate element can be applied, and it is shown that the track slab and bridge accelerations with modelling of the Mindlin-Reissner plate are slightly smaller than those by double-beam and thin-plate track slabs at specifically high frequency ranges.

(2) From the aspect of system stability, the longitudinally connected track slabs posse obvious advantages, and for discontinuous track slabs, the higher of the track slab spacing, the larger of the track-bridge dynamic displacements.

(3) The minimum length truncated before the first wheel and behind the last wheelset should be longer than the bridge span length in the system matrix truncation. What's more, the proposed matrices truncation method proves effective in boosting computational efficiency.

Disclosure statement

No potential conflict of interest was reported by the author(s).

Funding

This work was supported by the National Natural Science Foundation of China (Grant No.: 52008404; U1934217; 51708558), Science and Technology Research and Development Program Project of China Railway Group Limited (2020-Special-02).

References

- [1] Montenegro PA, Carvalho H, Ribeiro D, et al. Assessment of train running safety on bridges: a literature review. *Eng Struct.* 2021;241:112425.
- [2] Guo W, Xia H, De Roeck G, et al. Integral model for train-track-bridge interaction on the Sesia Viaduct: dynamic simulation and critical assessment. *Comput Struct.* 2012;112:205–216.
- [3] Xiao X, Yan Y, Chen B. Stochastic dynamic analysis for vehicle-track-bridge system based on probability density evolution method. *Eng Struct.* 2019;188:745–761.
- [4] Zhu Z, Gong W, Wang L, et al. An efficient multi-time-step method for train-track-bridge interaction. *Comput Struct.* 2018;196:36–48.
- [5] Lee YS, Kim SH, Jung J. Three-dimensional finite element analysis model of high-speed train-track-bridge dynamic interactions. *Adv Struct Eng.* 2005;8(5):513–528.
- [6] Zhai W, Han Z, Chen Z, et al. Train-track-bridge dynamic interaction: a state-of-the-art review. *Veh Syst Dyn.* 2019;57(7):984–1027.

- [7] Zhai W, Xia H, Cai C, et al. High-speed train-track-bridge dynamic interactions – part I: theoretical model and numerical simulation. *Int J Rail Trans.* 2013;1(1):3–24.
- [8] Zhai W, Wang S, Zhang N, et al. High-speed train-track-bridge dynamic interactions – part II: experimental validation and engineering application. *Int J Rail Trans.* 2013;1(1):25–41.
- [9] Yang Y, Yau J. Vehicle-bridge interaction element for dynamic analysis. *J Struct Eng.* 1997;123(11):1512–1518.
- [10] Yang Y, Yau J, Wu Y. *Vehicle-bridge interaction dynamics: with applications to high-speed railways.* Singapore: World Scientific Publishing; 2004.
- [11] Cheng Y, Au FTK, Cheung YK. Vibration of railway bridges under a moving train by using bridge-track-vehicle element. *Eng Struct.* 2001;23(12):1597–1606.
- [12] Lou P. vehicle-track-bridge interaction element considering vehicle's pitching effect. *Finite Elem Anal Des.* 2005;41(4):397–427.
- [13] Lou P, Yu Z, Au FTK. Rail-bridge coupling element of unequal lengths for analyzing train-track-bridge interaction systems. *Appl Math Modell.* 2012;36(4):1395–1414.
- [14] Yang H, Chen Z, Li S, et al. An integrated coupling element for vehicle-rail-bridge interaction system with a non-uniform continuous bridge. *Acta Mech Solida Sinica.* 2015;28(3):313–329.
- [15] Dai G, Yan B. Beam-track interaction of high-speed railway bridge with ballast track. *J Cent South Univ Technol.* 2012;19(5):1447–1453.
- [16] Xu L, Zhai W. A three-dimensional dynamic model for train-track interactions. *Appl Math Modell.* 2019;76:443–465.
- [17] Montenegro PA, Neves SG, Calçada R, et al. Wheel–rail contact formulation for analyzing the lateral train–structure dynamic interaction. *Comput Struct.* 2015;152:200–214.
- [18] Zhang N, Zhou Z, Wu Z. Safety evaluation of a vehicle–bridge interaction system using the pseudo-excitation method. *Railw Eng Sci.* 2022;30(1):41–56
- [19] Zhu Z, Tang Y, Ba Z, et al. Seismic analysis of high-speed railway irregular bridge–track system considering V-shaped canyon effect. *Railw Eng Sci.* 2022;30(1):57–70.
- [20] Neto J, Montenegro PA, Vale C, et al. Evaluation of the train running safety under crosswinds-a numerical study on the influence of the wind speed and orientation considering the normative Chinese Hat model. *Int J Rail Trans.* 2021;9(3):204–231.
- [21] Dinh VN, Kim KD, Warnitchai P. Dynamic analysis of three-dimensional bridge-high-speed train interactions using a wheel-rail contact model. *Eng Struct.* 2009;31(12):3090–3106.
- [22] Zeng Q, Dimitrakopoulos EG. Derailment mechanism of trains running over bridges during strong earthquakes. *Procedia Eng.* 2017;199:2633–2638.
- [23] Zeng Z, Liu F, Lou P, et al. Formulation of three-dimensional equations of motion for train-slab track-bridge interaction system and its application to random vibration analysis. *Appl Math Modell.* 2016;40(11–12):5891–5929.
- [24] Chen M, Sun Y, Zhai W. High efficient dynamic analysis of vehicle–track–subgrade vertical interaction based on Green function method. *Veh Syst Dyn.* 2020;58(7):1076–1100.
- [25] Xu L, Yu Z, Shi C. A matrix coupled model for vehicle-slab track-subgrade interactions at 3-D space. *Soil Dyn Earthq Eng.* 2020;128:105894.
- [26] Xu L, Xin L, Yu Z, et al. Construction of a dynamic model for the interaction between the versatile tracks and a vehicle. *Eng Struct.* 2020;206:110067.
- [27] Zhai W. *Vehicle–track coupled dynamics: theory and application.* Singapore: Springer; 2020.
- [28] Xu L. On dynamic analysis method for large-scale train-track-substructure interaction. *Railway Eng Sci.* 2022;30(2):162–182.

Appendix

Table A1. Bridge and track slab structure parameters.

Parameter	Definition	Value
$K_{sb,y}$	Track slab-girder lateral interaction stiffness	$4.0 \times 10^7 \text{N/m}$
$K_{sb,z}$	Track slab-girder vertical interaction stiffness	$6.6 \times 10^8 \text{N/m}$
w_s	Track slab width	2.5 m
l_s	Track slab element length	0.325 m
L_{sb}	Track slab length	5.6 m
H_b	Vertical distance between the girder centroid and track slab centroid	2.2 m
W_b	Lateral distance between the girder centroid and track slab centroid	5 m
l_{tb}	Beam elemental length of the girder	1.086 m
N_b	Total number of bridge spans	3
n_b	Finite elements numbers for each girder	30
L_{sb}	Total length of the track slabs before the starting of the bridge	100 m
l_r	Distance between adjacent rail pads	0.63 m
l_{ss}	Spacing of adjacent track slabs	0.1 m to 0.5 m
l_b	The minimum boundary length	Variable between 10 to 50 m
L_b	Bridge span length	32.6 m
$K_{bs,y}$	Ground-pier interaction Stiffness (y direction)	$1.0 \times 10^9 \text{N/m}$
$K_{bs,z}$	Ground-pier interaction Stiffness (z direction)	$1.0 \times 10^{10} \text{N/m}$
$C_{bs,z}/C_{bs,y}$	Ground-pier interaction Damping (y and z directions)	$5.0 \times 10^4 \text{N} \cdot \text{s/m}$

Table A2. Vehicle parameters.

Parameters	Values	Unit
Car body mass	45280	kg
Car body yaw moment of inertia	2.1399×10^6	$\text{kg} \cdot \text{m}^2$
Car body rolling moment of inertia	1.4997×10^6	$\text{kg} \cdot \text{m}^2$
Car body pitch moment of inertia	2.2678×10^6	$\text{kg} \cdot \text{m}^2$
Bogie mass	3300	kg
Bogie yaw moment of inertia	3300	$\text{kg} \cdot \text{m}^2$
Bogie rolling moment of inertia	2673	$\text{kg} \cdot \text{m}^2$
Bogie pitch moment of inertia	1807	$\text{kg} \cdot \text{m}^2$
Wheelset mass	1780	kg
Wheelset yaw moment of inertia	967	$\text{kg} \cdot \text{m}^2$
Wheelset rolling moment of inertia	949	$\text{kg} \cdot \text{m}^2$
Primary suspension longitudinal stiffness	1.468×10^7	N/m
Primary suspension lateral stiffness	6.47×10^6	N/m
Primary suspension vertical stiffness	1.04×10^7	N/m
Primary suspension vertical damping	9800	$\text{N} \cdot \text{s/m}$
Secondary suspension longitudinal stiffness	1.67×10^5	N/m
Secondary suspension lateral stiffness	1.67×10^5	N/m
Secondary suspension vertical stiffness	3.2284×10^5	N/m
Secondary suspension vertical damping	9800	$\text{N} \cdot \text{s/m}$
Bogie distance	17.5	m
Wheel distance	2.5	m